Journal of Physics: Conference Series **326** (2011) 012026 doi:10.1088/1742-6596/326/1/012026

TEM 3-beam study of annealing effects in InGaNAs using ab-initio structure factors for strain-relaxed supercells

K Müller[1], M Schowalter[1], O Rubel[2], D Z Hu[3], D M Schaadt[3], M Hetterich[3], P Gilet[4], R Fritz[5], K Volz[5] and A Rosenauer[1]

[1] Universität Bremen, Otto-Hahn-Allee 1, 28359 Bremen, Germany
[2] Thunder Bay Regional Research Institute, 290 Munro Street, Thunder Bay, Canada
[3] Karlsruhe Inst. of Technology, Wolfgang-Gaede-Str. 1, 76131 Karlsruhe, Germany
[4] CEA LETI Minatec Campus, 17 Av. des Martyrs, 38054 Grenoble Cedex 9, France
[5] Philipps Universität Marburg, Hans-Meerwein-Str., 35032 Marburg, Germany

Abstract. We report on a Transmission Electron Microscopy 3-beam technique based on the interference of 000, 200 and 220. Nonlinear imaging artefacts are eliminated by Fourier filtering, yielding 200 and 220 lattice fringe images, from which chemically sensitive contrast and strain are measured, respectively. In this way, In and N composition can be mapped at atomic scale in quaternary InGaNAs by comparison with simulated reference data. Our Bloch wave simulations are based on structure factors derived from supercells with 10^6 atoms, which have been strain-relaxed by valence force field methods. Additionally, the influence of electron redistributions due to chemical bonding is accounted for by modified atomic scattering amplitudes derived from density functional theory. By comparing local compositions in an annealed $In_{0.28}Ga_{0.72}N_{0.025}As_{0.975}$ sample with its as-grown counterpart, we find homogenisation of InGaNAs layer thickness and –stoichiometry upon annealing.

1. Introduction

Due to their potential for near-infrared signal transmission in optical fibres, dilute nitrides such as quaternary $In_xGa_{1-x}N_yAs_{1-y}$ are intensely studied for more than a decade. As to the optical properties of InGaNAs, room temperature photoluminescence (PL) in the desired spectral range at wavelengths of 1.3 and 1.55μm can indeed be realised, but PL peaks are very weak and broad. Common to most reports is the observation of a drastic increase of PL intensity accompanied by a blue-shift of several tens of nanometres after thermal annealing [1]. To explain this behaviour, enormous theoretical effort has been spent on studying responsible atomic-scale scenarios, of which the most prominent either focus on long-range diffusion processes [2,3] or modifications of preferential coordinations of In and N atoms [1,4]. However, it is difficult to clarify this issue from the experimental point of view with available transmission electron microscopy (TEM) techniques, because unique atomic-scale mapping of both local In and local N concentration is necessary.

In the following, we firstly introduce a TEM technique which exploits local chemically sensitive contrast and local strain contained in an image formed by the beams 000, 200 and 220. In this way, subsequent superposition of two images taken under different specimen tilts [5] is avoided to assure availability of strain and contrast from the same position. Because accurate simulations for the 200 fringe amplitude are required as reference data, we secondly report on modelling InGaNAs structure

[1] Any correspondence should be addressed to Knut Müller (mueller@ifp.uni-bremen.de).

factors in order to include chemical bonding via modified atomic scattering amplitudes (MASA) obtained from density functional theory (DFT), as well as static atomic displacements (SAD) via valence force field (VFF). Thirdly, thermal annealing effects on $In_{0.28}Ga_{0.72}N_{0.025}As_{0.975}$ are studied using the 3-beam imaging method and reference data accounting for bonding and SAD.

2. The three-beam imaging method

An L-shaped objective aperture has been fabricated in a focused ion beam facility from a 7 µm Pt-foil and was inserted in an FEI Titan 80/300 equipped with an aberration corrector for imaging. The method is summarised in Fig. 1. The aperture shown in Fig. 1a leads to the 3-beam image shown in Fig. 1b. As can be seen in the diffractogram in Fig. 1c, 220, 200 and 020 fringes occur, the latter being caused by nonlinear imaging.

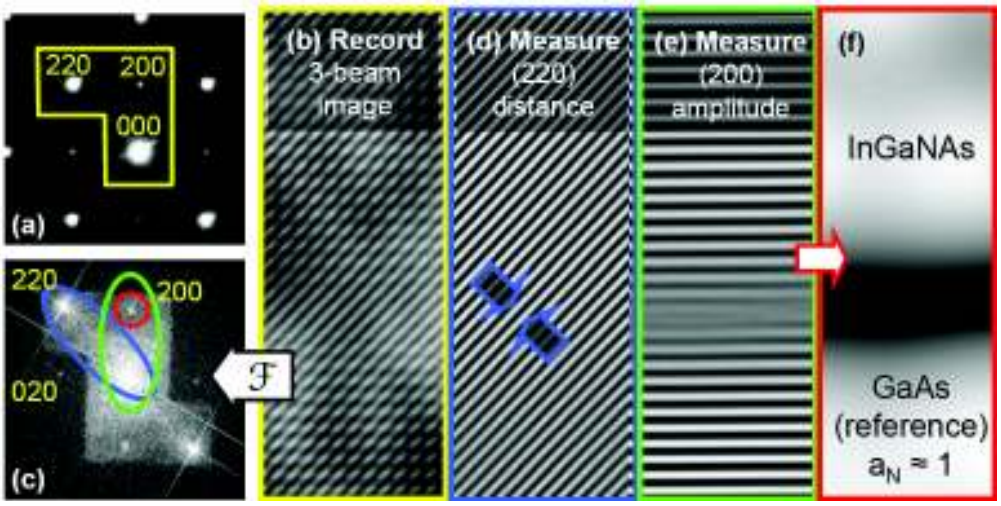

Figure 1. Formation and evaluation of TEM 3-beam images. (a) FIB-aperture in diffraction plane. (b) 3-beam image taken with Laue circle centre at (0 4.2 0). (c) Diffractogram. (d) 220 and (e) 200 lattice planes constructed from (b,c). (f) 200 fringe amplitude a_N showing an InGaNAs/GaAs interface.

Using beams $\mathbf{g_1} = (000), \mathbf{g_2} = (200)$ and $\mathbf{g_3} = (220)$, the image intensity reads

$$I = A_1^2 + A_2^2 + A_3^2 + 2A_1A_2T_{12}\cos(2\pi\mathbf{g}_2\mathbf{r} - \phi_{12} - \varphi_{12}) + 2A_1A_3T_{13}\cos(2\pi\mathbf{g}_3\mathbf{r} - \phi_{13} - \varphi_{13}) + 2A_2A_3T_{23}\cos(2\pi(\mathbf{g}_2 - \mathbf{g}_3)\mathbf{r} - \phi_{23} - \varphi_{23}), \quad (1)$$

where $A_n \exp(i\varphi_n)$ is the amplitude of diffracted beam $\mathbf{g}_n$, $\varphi_{nm} = \varphi_n - \varphi_m$ is the phase difference between beams $\mathbf{g}_n$, $\mathbf{g}_m$ and $T_{nm}\exp(i\phi_{nm})$ is the corresponding transmission cross coefficient. Hence the occurrence of the 020 reflection in Fig. 1c is the only nonlinear contribution, meaning that amplitudes and phases of the other diffractogram reflections are equal to the respective two-beam results. Indeed, including any further diffracted beam in the imaging process would impose its thickness dependence on amplitudes and phases of the 200 and 220 fringes, making their interpretation more complicated or impossible in case specimen thickness is inaccurately known. However, according to Figs. 1d and 1e, two-beam 220 and 200 lattice fringe images can be obtained by Fourier filtering, the former providing strain and the latter chemically sensitive contrast. Note that strain data is available also at the minimum of the 200 fringe amplitude. As indicated in Fig. 1f, the 200 fringe amplitude is normalised to a background fitted to regions with known composition.

Figures 1d and 1f define both strain and amplitude for each lattice point, as depicted on the left of Fig. 2. Together with the simulated counterparts, this defines an intersection of an isostrain and an isoamplitude contour in the reference data on the right of Fig. 2, yielding both local In content x and

local N content *y*. Reference 200 fringe amplitudes correspond to Bloch wave simulations [6] with a Laue circle centre at (0 4.2 0), for which the thickness dependence was found to be minimal.

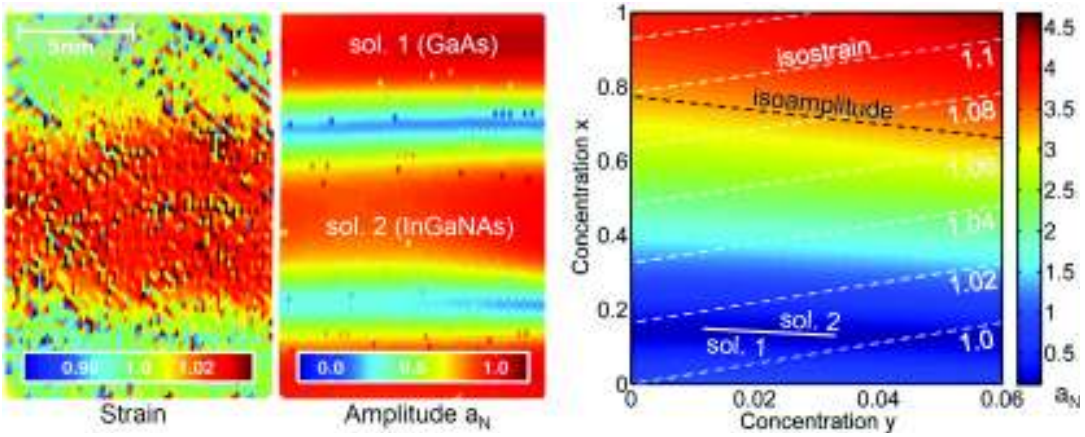

Figure 2. *Left:* Normalised fringe distance and amplitude determined from Figs. 1d, f. *Right:* Simulation of strain (dashed white isolines) and normalised 200 fringe amplitude a_N (colour).

3. Modelling bonding and SAD effects on electron structure factors

Even in binary GaAs and InAs electron redistribution due to chemical bonding severely affects low-order structure factors such as 200, so that it must definitely be taken into account in InGaNAs alloys. However, differences in atomic radii of N and In with respect to atoms of the host sublattices cause SAD. These are usually taken into account by considering supercells with about 10^6 atoms and performing VFF calculations. Since bonding is typically treated by DFT which applies to cells with about 10^2 atoms only, bonding effects need to be modelled.

For the Bloch wave simulations in Fig. 2 we used atomistic modelling of bonding based on MASA. These are indeed calculated by DFT, but only for all *binary* zinc-blende compounds that can be constructed from $In_xGa_{1-x}N_yAs_{1-y}$. Composition dependence and thin foil relaxation are introduced by calculating MASA from tetragonally distorted Bravais cells. For details, see Refs. [7,8]. In the latter report, we found that SAD from VFF are accurate to a few picometres, being less than mean thermal vibrational amplitudes. It was furthermore pointed out that, for supercells with 216 atoms, modelling bonding by MASA and SAD by VFF is in good agreement with full DFT calculations. However, large errors in structure factor amplitudes and phases may result if neglecting bonding and SAD.

The actual procedure for calculating structure factors is explained in Fig. 3.

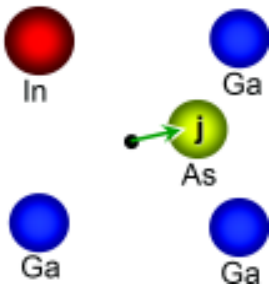

Figure 3. Schematic to demonstrate the treatment of bonding and SAD for structure factor calculation. First, large supercells (10^6 atoms) are strain-relaxed using VFF calculations. Second, structure factors are calculated for this cell. The MASA at lattice site *j* is modelled by determining nearest neighbours, defining the type of (binary) bonds involved. In the example on the left, As at site *j* has the MASA

$$f_{As,j}^{InGaNAs}(\mathbf{g}) = \tfrac{1}{4}[f_{As}^{InAs}(\mathbf{g}) + 3f_{As}^{GaAs}(\mathbf{g})] \ ,$$

as 3 bonds of type As in GaAs and one of type As in InAs are present.

4. Annealing effects on $In_{0.28}Ga_{0.72}N_{0.025}As_{0.975}$

The 3-beam method in combination with reference data from the previous section has been applied to an $In_xGa_{1-x}N_yAs_{1-y}$ sample with nominal contents $x = 0.28$ and $y = 0.025$ before and after thermal annealing for 15 min under N_2 atmosphere at 600K. The PL of the annealed sample is shifted by 65nm towards smaller wavelengths and 20 times more intense. Composition maps and profiles are depicted

in Fig. 4, exhibiting island formation in the as-grown sample. Inside the island, In enrichment of 0.03-0.05 is found, being anticorrelated to an N enrichment of 0.02-0.03 outside. In contrast, nearly homogeneous layer thickness and –stoichiometry is found after annealing. Error bars in Fig. 4c correspond to statistical lateral fluctuations, whereas the grey corridor indicates the error introduced by inaccurately known specimen thickness. As-grown profiles in Fig. 4f show both anticorrelation of In and N content as well as changes in InGaNAs layer thickness with respect to positions A, B in Fig. 4d.

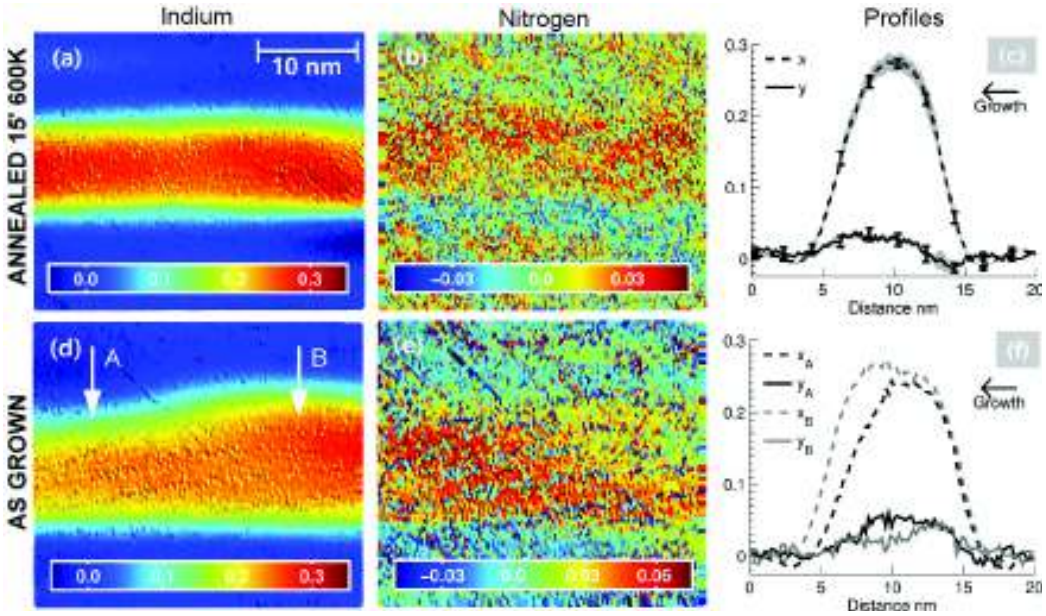

Figure 4. (a-c) In and N contents after annealing. The grey corridor in (c) includes all evaluations for thicknesses between 10 and 80 nm. (d-f) In and N contents for the as-grown counterpart. Profiles in (f) are taken at paths indicated in (d).

5. Conclusions

TEM 3-beam imaging can be used to subsequently recover 200 and 220 2-beam lattice fringe images for which linear imaging theory applies. Both chemically sensitive amplitude and strain can thus be measured independently, enabling atomic-scale concentration mapping in quaternary (zinc-blende) alloys by comparison with strain and amplitude reference data. The latter includes bonding via DFT-MASA and SAD from VFF. Disappearance of In-N anticorrelations in an $In_{0.28}Ga_{0.72}N_{0.025}As_{0.975}$ layer after annealing suggests that both long-range diffusion and increase of the frequency of In-N bonds ought to be responsible for a blue-shift of 65 nm observed in PL spectra in this study.

References

[1] Klar P J et al. 2001 *Phys. Rev. B* **64** 121203.
[2] Djie H S, Wang D-N, Ooi B S, Hwang J C M, Fang X M, Wu Y, Fastenau J M, Liu W K 2007 *Thin Solid Films* **515**(10) 4344-4347.
[3] Peng C S, Pavelescu E M, Jouhti T, Konttinen J, Pessa M 2003 *Solid-State Electronics* **47**(3) 431-435.
[4] Jenichen A, Engler C, Leibiger G, Gottschalch V 2005 *Surface Science* **574**(2-3) 144-152.
[5] Grillo V, Albrecht M, Remmele T, Strunk H P, Egorov A Y, Riechert H 2001 *Journal of Applied Physics* **90**(8) 3792-3798.
[6] Müller K, Schowalter M, Jansen J, Tsuda K, Titantah J, Lamoen D, Rosenauer A 2009 *Ultramicroscopy* **109** 820-814.
[7] Rosenauer A, Schowalter M, Glas F, Lamoen D 2005 *Phys. Rev. B* **72** 085326.
[8] Müller K, Schowalter M, Rosenauer A, Rubel O, Volz K 2010 *Phys. Rev. B* **81** 075315.
[9] This work was supported by the DFG under contracts RO 2057/4, SCHO 1196/3 and VO 805/4,5.